Biosensors and Bioelectronics 315 (2027) 119220

Contents lists available at ScienceDirect

Biosensors and Bioelectronics

journal homepage: www.elsevier.com/locate/bios

Rational design of a fluorescent probe for selective sensing of human cytochrome P450 2C19 and its application in exploration of enzymatic inactivation

Zhenhao Tian [a,1], Fei Yan [a,1], Yichao Su [b,1], Xiaoren Zhang [c], Jiayue Wang [d], Jianing Xiao [b], Yifei Dang [b], Jing Ning [b,*], Lei Feng [a,e,**], Chengjuan Xing [a], Xiaohong Shu [b], Jingnan Cui [f], Tony D. James [e,g], Xiaochi Ma [a,h,***]

[a] The Second Affiliated Hospital, Dalian Medical University, Dalian, 116023, China
[b] College of Pharmacy, Dalian Medical University, Dalian, 116044, China
[c] Weifang University of Science and Technology, Shandong, 262700, China
[d] Beijing DP Technology Co., Ltd., Beijing, 100080, China
[e] School of Chemistry and Chemical Engineering, Henan Normal University, Xinxiang, 453007, China
[f] State Key Laboratory of Fine Chemicals, Dalian University of Technology, Dalian, 116024, China
[g] Department of Chemistry, University of Bath, Bath, BA2 7AY, United Kingdom
[h] Heilongjiang University of Chinese Medicine, Harbin, 150040, China

ARTICLE INFO

Keywords:
Cytochrome P450 2C19
Rational molecular design
Irreversible inactivators
Analytical methods
Fluorescent probes

ABSTRACT

Human cytochrome P450 2C19 (CYP2C19) is a drug-metabolizing enzyme frequently implicated in adverse drug reactions. However, the identification of inhibitors, especially irreversible inactivators, that underlie CYP2C19-mediated drug interactions remains challenging, chiefly owing to the paucity of robust molecular probes capable of quantification of enzymatic inactivation profiles in biospecimens. In the present study, we propose a molecular modification strategy that fine-tunes unfavorable substrate–aromatic interactions within the CYP2C19 pocket by rationally modifying a key junction domain of **B1**, a substrate that currently suffers from sub-optimal selectivity and sensitivity. The optimized probe **BCPM** exhibits 20-fold selectivity over other CYP isoforms and a detection limit of 0.012 nM. A dual-mode visual platform was developed that enables screening and mechanistic elucidation of reversible inhibitors and inactivators of CYP2C19 among drugs and natural products. Using this platform, we thoroughly validated the multifaceted inhibitory effects of representative compounds on CYP2C19, as well as the potential for adverse drug interactions resulting from enzyme inactivation. Collectively, our rationally fine-tuned structural strategy generated a robust tool for CYP2C19 with broad utility in biomedical and pharmaceutical research.

1. Introduction

Cytochrome P450s (CYP) are heme-containing catalysts involved in the metabolism of therapeutic drugs, xenobiotics and endogenous substance (Rendic and Guengerich, 2015; Guengerich, 2024; Roichman et al., 2025). Human CYP2C19 enzyme constitutes 16% of the human CYP2C proteins in the liver, and is responsible for the metabolism of approximately 15% of marketed drugs (Evans and Relling, 1999; Goldstein, 2001; Ford and Taubert, 2013; Thuy et al., 2026). Proton pump inhibitors such as omeprazole and pantoprazole, benzodiazepine and psychotropic drugs such as diazepam, and platelet aggregation inhibitor such as clopidogrel are all drug substrates of CYP2C19.

The clinical significance of CYP2C19 has been well documented (Berge et al., 2011; Zanger and Schwab, 2013; Jiang and You, 2015; Fricke-Galindo et al., 2016; Mu et al., 2025). One of the concerns is the frequent occurrence of variability in the pharmacokinetics of various

* Corresponding author. College of Pharmacy, Dalian Medical University, Dalian, 116044, China.
** Corresponding author. The Second Affiliated Hospital, Dalian Medical University, Dalian, 116023, China.
*** Corresponding author. The Second Affiliated Hospital, Dalian Medical University, Dalian, 116023, China.
E-mail addresses: ningjing0626@163.com (J. Ning), leifeng@dmu.edu.cn (L. Feng), maxc1978@163.com (X. Ma).
[1] These authors contributed equally to this work.

https://doi.org/10.1016/j.bios.2026.119220
Received 10 April 2026; Received in revised form 29 August 2026; Accepted 9 September 2026
Available online 10 September 2026
0956-5663/© 2026 Elsevier B.V. All rights are reserved, including those for text and data mining, AI training, and similar technologies.

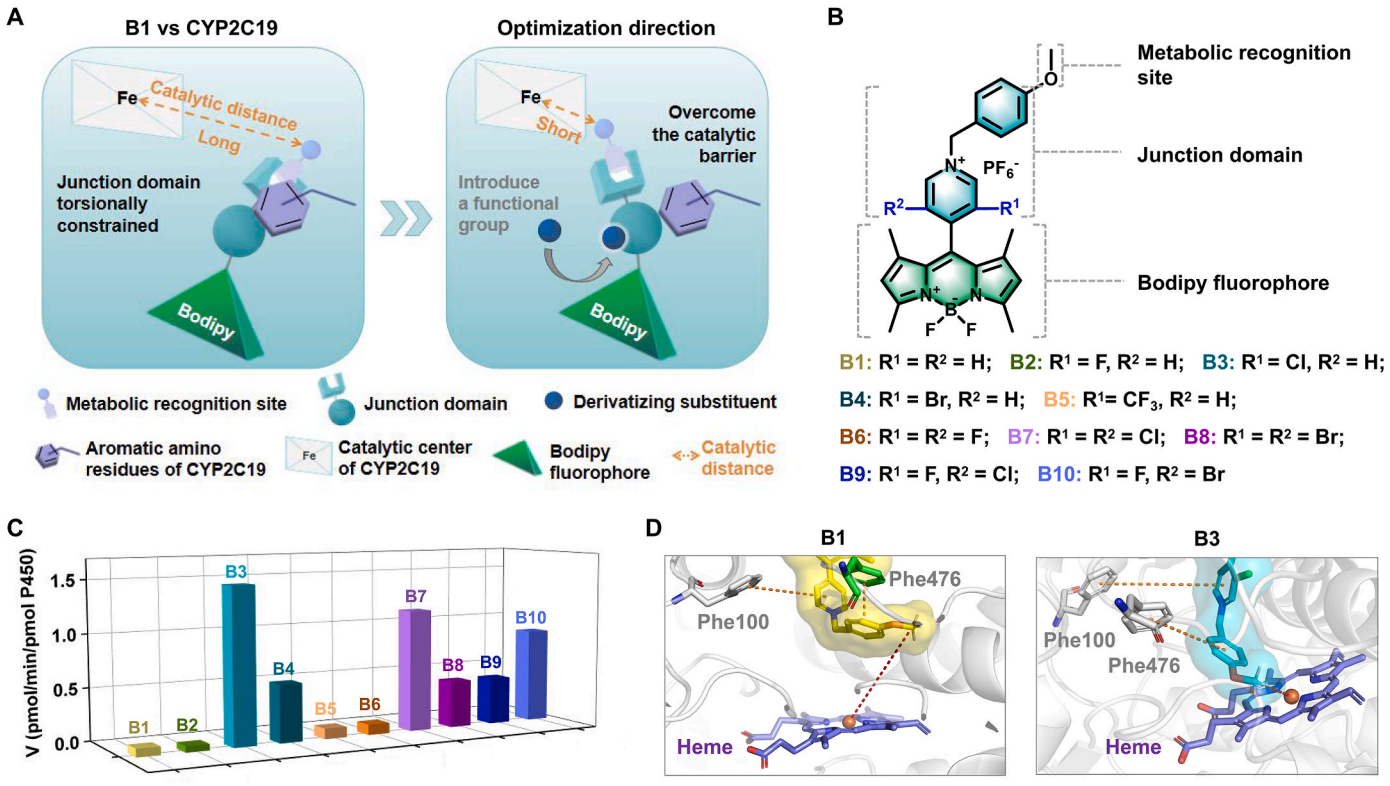


Fig. 1. Fine-tuning unfavorable substrate-enzyme interactions to rationally design a fluorescent probe for CYP2C19. (A) The schematic depicts (left) substrate **B1** bound in the CYP2C19 pocket, interacting with neighboring aromatic residues and featuring constrained torsional flexibility; and (right) the ideal conformation that achieves localized flexibility and reduces the catalytic distance. (B) The metabolic recognition site, intermediate junction domain and Bodipy fluorophore domain of **BCM** derivatives (**B1**-**B10**). (C) Rate of CYP2C19-mediated metabolism of **BCM** derivatives. (D) Docking simulation of **B1** and **B3** into CYP2C19, showing the distances from the metabolic recognition sites of **B1** and **B3** to the catalytic center of CYP2C19 and junction domain of **B1** and **B3** to aromatic residues Phe476 and Phe100, respectively.

clinically drugs metabolized by CYP2C19 (Desta et al., 2002; Li et al., 2026). The CYP2C19 gene is highly polymorphic, and specific genotypes contribute to substantial inter-individual variability in drug metabolism (Mega et al., 2009; Wallentin et al., 2010; Byoun et al., 2026). Additionally, CYP2C19 is high susceptible to metabolic drug interactions owing to its broad substrate-spectrum (Sychev et al., 2018; Gougis et al., 2021). The modulatory effects of drugs can increase the variability of CYP2C19 activity among individuals, which is a key causative factor leading to potential clinical safety issues (Harmsze et al., 2011; Furuta et al., 2010).

The activity modulatory effects of small molecules on metabolic targets such as CYP2C19 can be classified into direct and indirect modes of action, which correspond to reversible and irreversible inhibition, respectively (Lin and Lu, 1998; Lee et al., 2012; Guengerich, 2020). Notably, indirect enzymatic inhibition is usually based on new substances formed that exhibit a stronger inhibitory effect. And in many cases, a highly reactive intermediate is formed, which could covalently modify key residues in the enzyme active site leading to the irreversible dysfunction of the enzyme, termed mechanism-based inactivation (Kalgutkar et al., 2007; Tang et al., 2022; Zhou et al., 2022). Notably, indirect and metabolism-dependent inhibition is difficult to detect and accurately predict, and more importantly, it is frequently associated with metabolism-based drug interactions and adverse effects of drugs. As such, research effort should focus on the discovery and characterization of metabolism-activated small molecule inhibitors, yet these studies have been hampered by a lack of powerful tools for rapidly recognize inhibitors from natural systems and reliably sense the real-time activity fluctuations of CYP2C19 that signify its inactivation within complex bio-systems.

Small molecule based fluorescent probes enable non-invasive visualization and high-throughput analysis of biomolecules, offering high detection sensitivity and high-resolution imaging capabilities (Wu et al., 2022; Yan et al., 2022; Grasso et al., 2023; Cheng and Pu, 2024; Chen et al., 2026; Cedrún-Morales et al., 2026; Wang et al., 2026). Given the pivotal role of CYP enzymes in the metabolism of both exogenous and endogenous compounds, and their consequent impact on clinical efficacy and safety, a diverse array of highly selective fluorescent probes has been developed. These probes have served as essential tools for the rapid discovery of reversible and irreversible CYP isoform inhibitors and for the elucidation of metabolism-mediated drug-drug interactions (Feng et al., 2021, 2022; Ning et al., 2022, 2024; He et al., 2023; Xu et al., 2026). Thus far, a few fluorescent probes have been reported for the sensing of CYP2C19 activity, e. g. coumarin or fluorescein derivatives (Donato et al., 2004; Sudsakorn et al., 2007; Salminen et al., 2011; Juvonen et al., 2019). However, these fluorescent probes exhibit low sensitivity and poor selectivity to CYP2C19 (Table S1). For example, the reported 3-*O*-methylfluorescein (3 MF) also displayed a high response to CYP1A1, with an approximately 3.3-fold higher selectivity for CYP2C19 than for CYP1A1 (Sudsakorn et al., 2007). The sub-optimal selectivity of these reactive fluorescent substrates substantially constrains their practical applicability, making them unsuitable for activity imaging in cells, tissues, and other complex biological specimens, let alone dynamic analysis of the activity of CYP2C19 in living system. Consequently, there is a pressing need to develop versatile, high-performance fluorescent probes for CYP2C19.

CYP subfamily 1, 2 and 3 have numerous members that involved in the metabolism of therapeutic drugs and other xenobiotics (Feng et al., 2021; Yang et al., 2025). Although most isoforms exhibit a certain degree of substrate specificity, substrate overlap is still substantial, exemplified by the commonly reported co-substrates for CYP2C19 and

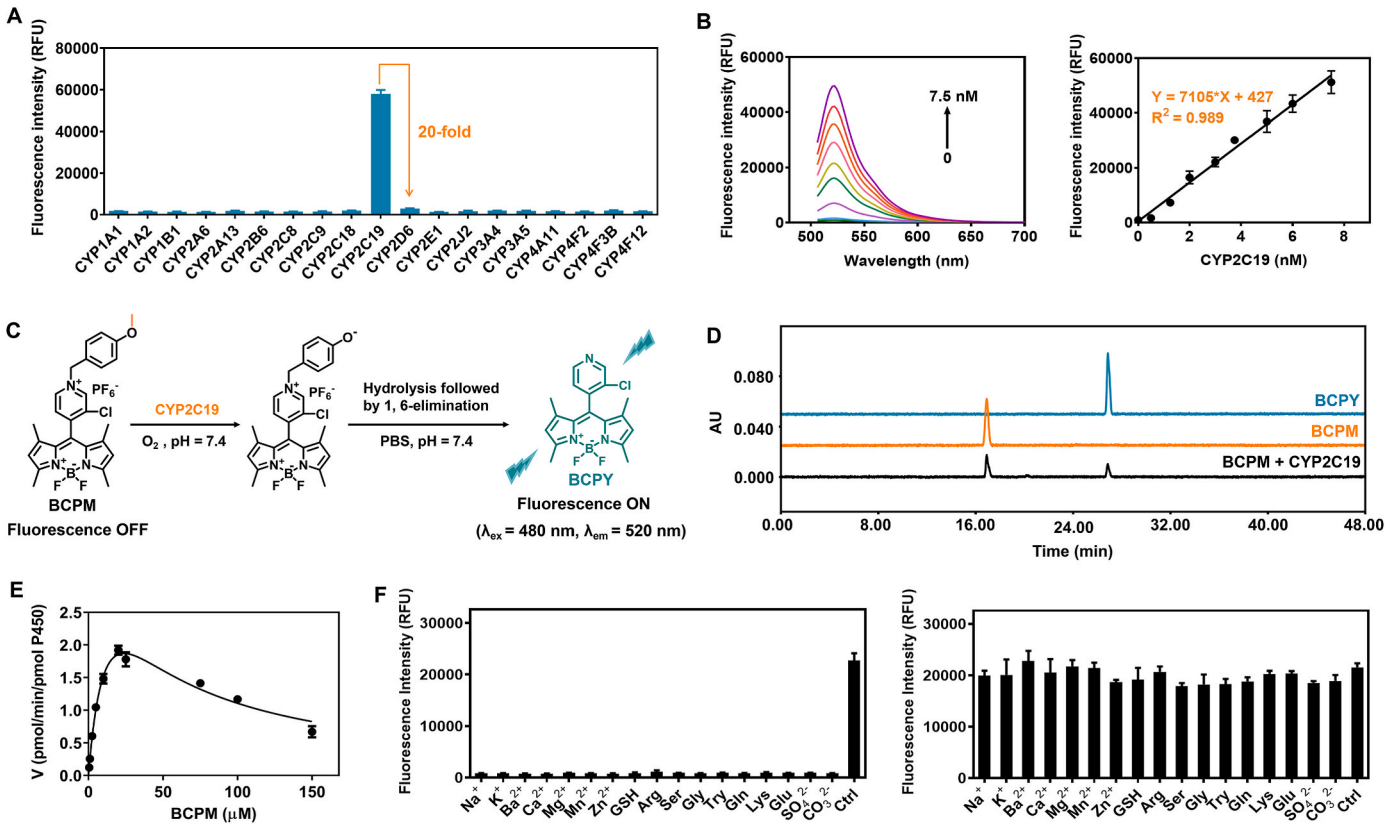


Fig. 2. Fluorescence response of **BCPM** toward CYP2C19. (A) Fluorescence intensity at 520 nm of **BCPM** (10 μM) when incubating with various human CYP subtypes (10 nM) for 60 min. (B) Fluorescence spectra and gradually increasing fluorescence intensity at 520 nm of **BCPM** (10 μM) when incubated with increasing concentrations of CYP2C19 (0-7.5 nM) for 60 min. (C) Proposed mechanism of CYP2C19 triggering the fluorescence response of **BCPM**. (D) HPLC chromatograms of CYP2C19-incubated reaction mixtures and authentic standards of **BCPM** and **BCPY**. (E) Kinetic plots of **BCPY** formation catalyzed by CYP2C19. (F) The evaluation of the influence of potential interfering substances on the fluorescence response of **BCPM** (10 μM) in the absence (Left) or presence (Right) of CYP2C19. The *in vitro* incubation experiments were conducted using a NADPH-generating system in buffer (pH 7.4). The relative fluorescence intensity is shown as the mean ± SD (n = 3).

CYP2C9 (Boyle et al., 2024), CYP2C19 and CYP2D6 (Hicks et al., 2013, 2017), CYP3A4 and CYP3A5 (Williams et al., 2002; Niwa et al., 2008). It is inherently challenging to develop a selective probe substrate for a target CYP isoform because there is usually overlapping metabolism among various CYP isoforms.

Therefore, unguided derivatization and modification of the fluorophore, that focusing exclusively on the alteration of the metabolic recognition moiety, are clearly insufficient for developing highly selective probes, such as the reported several CYP2C19 fluorescent probes (Table S1). The key issues for the development of selective fluorescent probes for CYP2C19 or other specific CYP isoforms were to propose a rational modification strategy, especially considering the interaction between fluorescent substrate and enzymes. It is necessary to thoroughly analyze the metabolic characteristics and interaction profiles between the small-molecule fluorescent ligand and the target enzyme, as well as the core factors that restrict or promote catalysis. On this basis, targeted and precise structural modifications should be implemented, followed by practical optimization of the molecular structure, to improve the compatibility between the fluorescent substrate and the target enzyme, and ultimately achieve rational optimization of the probe.

In the present study, by pinpointing the critical factors that hinder catalysis of CYP2C19 to the potential seed fluorescent substrate **B1**, we proposed a local conformational flexibility tuning strategy to implement the localized and precise optimization. Eventually, rational optimization and design of the CYP2C19 probe was realized, and the candidate probe **B3** (**BCPM**) exhibits enhanced compatibility with CYP2C19 and high selectivity toward CYP2C19.

2. Experimental

All reagents, materials, instruments, and experimental procedures are detailed in the Supporting Information.

3. Results and discussion

3.1. Molecularly induced flexibility tuning strategy to construct a fluorescent probe

As discussed above, the development of highly selective fluorescent probes for target enzymes is particularly challenging, largely due to the usually substrate overlap and inherent similarity among various CYP isoforms. More critically, even when a fluorophore successfully accesses the active site, its enzymatic response can be severely undermined by unfavorable metabolic factors. These obstacles constitute the critical bottlenecks hampering the development of highly selective probes for CYP2C19 and its relative isoforms (Feng et al., 2021). In previous studies, we found that **B1** can be recognized and catalyzed by CYP2C19, indicating the possibility of **B1** as a CYP2C19 fluorescent substrate (Ning et al., 2024). However, the response rate of **B1** to CYP2C19 was very low, and in addition responds to CYP2D6 which makes **B1** unsuitable to specifically monitor CYP2C19 activity in complex bio-samples. Thus, although challenging, we attempted to weaken the unfavorable factors and improve the catalytic compatibility of the fluorescent substrate with CYP2C19 to achieve a rational and precise modification of **B1** and develop a selective fluorescent probe for CYP2C19.

To uncover key restrictive factors for the catalytic reaction, **B1** was divided into three domains according to functional roles, including the

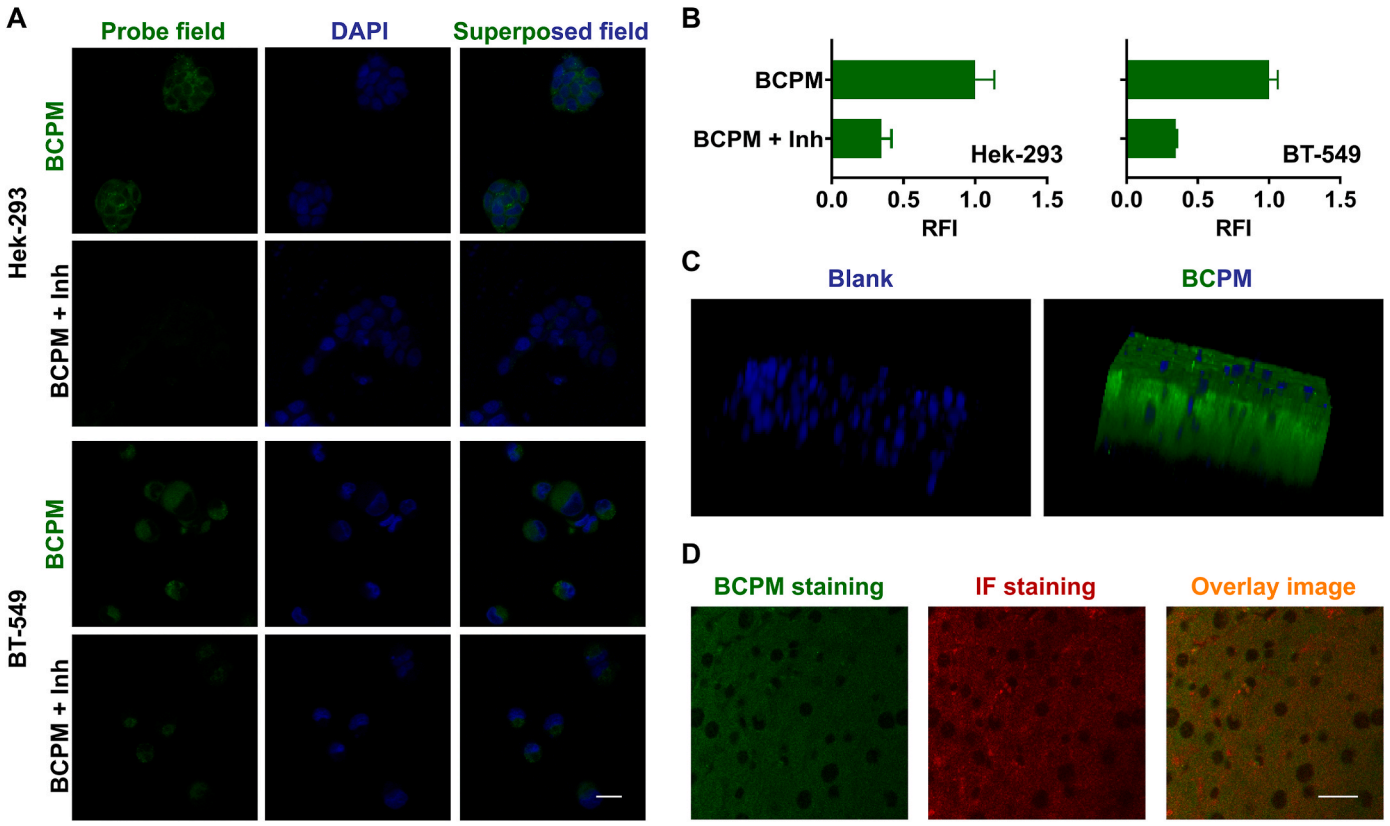


Fig. 3. Bioimaging of CYP2C19 in cells and tissues using **BCPM**. (A) Bioimaging of CYP2C19 in live cells using **BCPM** and (B) the relative fluorescence intensity (RFI) in the absence or presence of CYP2C19 inhibitor (Inh). (C) 3D images of CYP2C19 in mouse liver slices using **BCPM**. (D) Fluorescence (green) and immunofluorescence (IF, red) images of CYP2C19 in mouse liver slices. Imaging for CYP2C19, excitation: 488 nm, emission: 510 - 540 nm; immunofluorescence imaging, excitation: 633 nm, emission: 660 - 690 nm. The scale bar is 25 μm. (For interpretation of the references to colour in this figure legend, the reader is referred to the Web version of this article.)

methoxy group as metabolic recognition site, Bodipy fluorophore, and the intermediate junction domain (Fig. 1B). The amino-terminal residues involved in substrate binding were analyzed and indicated that the junction domain of **B1** exhibits strong interactions with Phe476 and Phe100 through π-π interactions (Fig. 1D), was the prominent contributions of aromatic residues in **B1** binding with CYP2C19 (Figs. S1 and S2). It was construed that the strong interaction with these aromatic residues greatly restricted the torsion of **B1** and thus hinders the metabolic recognition site getting closer to the catalytic center of CYP2C19 (Fig. 1A). The distance between the metabolic site of **B1** and the catalytic active center of CYP2C19 was estimated to be 10.1 Å, which confirmed our speculation. Therefore, we targeted the non-metabolic junction domain of **B1** for modification to enable greater torsional freedom and disrupt its interaction with nearby aromatic residues in CYP2C19, thereby shortening the catalytic distance and improving metabolic activity (Fig. S1).

Significantly, the space of the active cavity near the heme is relatively small, which prompted us to perform structural modification on the pyridine ring rather than the benzene ring that was closer to the methoxy group metabolic recognition site. Subsequently, a series of halogen atoms such as F and Cl were introduced into the pyridine ring of **B1** to build a focused library of potential substrates for CYP2C19 (Fig. 1B). The CYP2C19 activity assay demonstrated that among the derivatives (**BCM**), **B3** with Cl substituent exhibited a high reaction rate (Fig. 1C).

It was found that a longer distance between the aromatic residues of CYP2C19 and the junction domain of **B3** was observed compared with that of **B1**, which was attributed to the introduction of the Cl weakening the interaction between Phe100/Phe476 and the junction domain of the pro-fluorescent substrate. Most notably, the catalytic distance for **B3** was shortened to 6.5 Å, and the catalytic rate of **B3** was 18.6-fold higher than that of **B1** (Fig. 1C and D). This local chemical modification reduced the locking effect of Phe100 to the pyridine ring and fully restored the freedom of the benzene ring and the connected methoxy group metabolic site, thereby enabling the recognition site to access the catalytic active center of CYP2C19 (Fig. 1A). The results described above indicate that our chemical modification eliminated the restraining factors for catalytic reaction.

3.2. *Spectral response of probe BCPM*

We therefore focused on **B3** (**BCPM**) for subsequent investigations. Initially, the specificity of **BCPM** for CYP2C19 was confirmed *via* a variety of enzymatic assays. As shown in Fig. 2A, human CYP2C19 triggered a distinct fluorescence enhancement of **BCPM** at 520 nm, over other CYP subtypes. The high specificity of **BCPM** for CYP2C19 in complex tissue samples, such as human liver microsomes, was verified given that the 'Switch-ON' of **BCPM** was selectively inhibited by fluoxetine (a potent CYP2C19 inhibitor) (Fig. S3). When **BCPM** was incubated with CYP2C19, the fluorescence intensity at 520 nm was increased (Fig. 2B) and exhibited a increasing linear trend when CYP2C19 was added from 0 to 7.5 nM. The fluorescence OFF-ON switching mechanism of **BCPM** was attributed to 1, 6-elimination that was triggered by CYP2C19-mediated *O*-demethylation. The fluorescent metabolite of **BCPM** was identified as **BCPY**, by comparison with standard compounds, which confirmed that CYP2C19-mediated metabolic process promoted the 'Turn-ON' of **BCPM** (Fig. 2C and D).

The metabolism of **BCPM** exhibited substrate inhibition kinetics (Fig. 2E), and the K_m and V_{max} values of CYP2C19 were determined as 15.7 ± 4.2 μM and 4.32 ± 0.73 pmol/min/pmol P450 in the

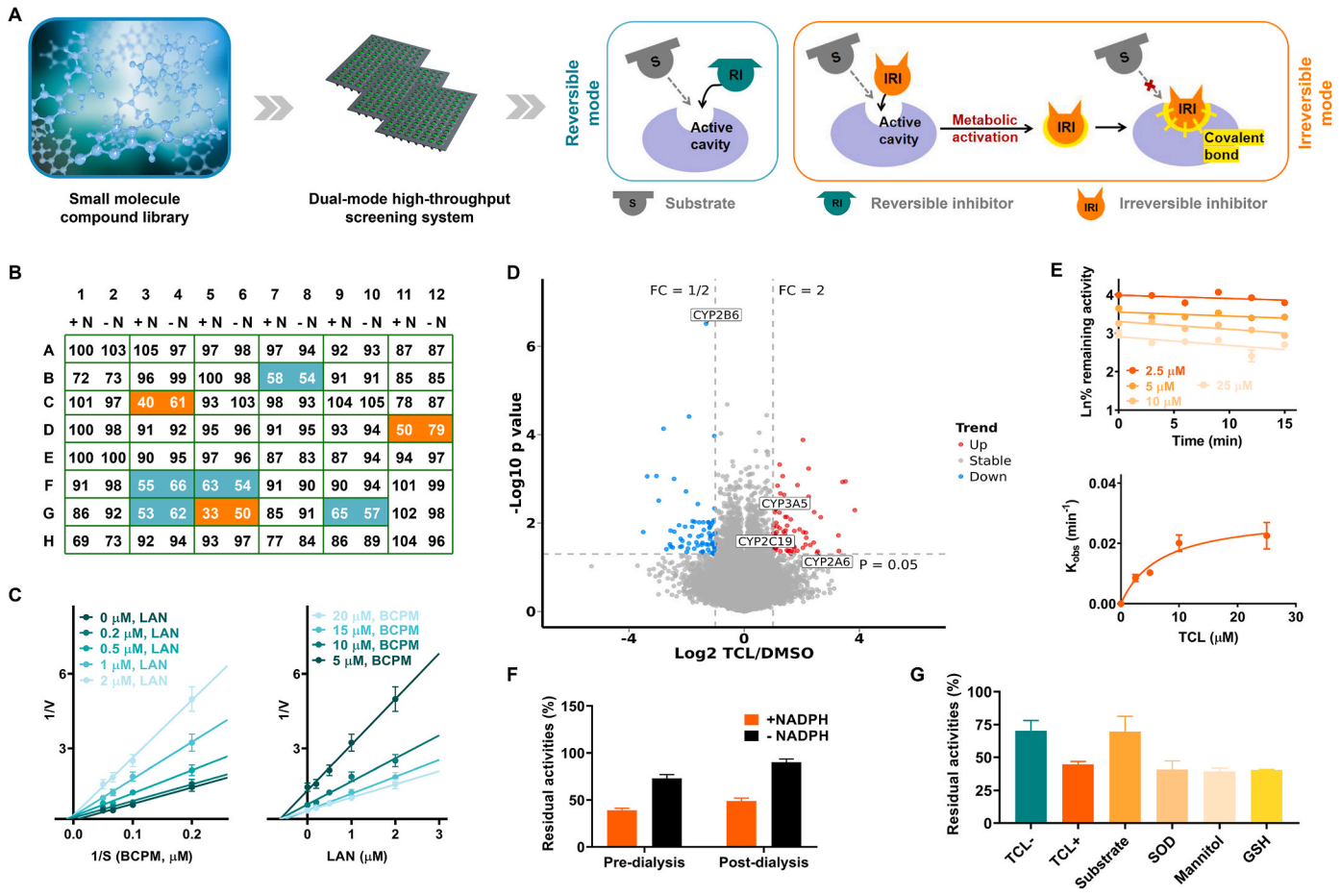


Fig. 4. Screening of reversible and metabolism-dependent irreversible inhibitors for CYP2C19. (A) Flowchart for the visual screening and characterization of reversible inhibitors (RI) and irreversible inhibitors (IRI). (B) Quantitative analysis of the inhibitory effect of drugs and natural products in 96-well microplates images (n = 3). The samples in the same row of the two adjacent columns represent screened compound that were pre-treated with (+N) or without NADPH (-N), respectively. The samples in $F_{11,12}$, $G_{11,12}$ and $H_{11,12}$ were the control treated with DMSO solvent. (C) Kinetic study of reversible inhibition of CYP2C19 by lansoprazole (LAN). (D) Volcano plot of the limited proteolysis-coupled mass spectrometry (Lip-MS) analysis of human liver microsomes samples treated with ticlopidine (TCL) or solvent control. (E) Kinetic study of irreversible inhibition of CYP2C19 by TCL. (F) Effect of dialysis on the irreversible inhibition of CYP2C19 by TCL. (G) Effects of potential protective agents upon the irreversible inhibition of CYP2C19 by TCL. TCL+/−, pre-metabolism with or without NADPH; GSH, glutathione; SOD, superoxide dismutase.

recombinant enzymatic activity assay (Table S2). A strong fluorescence signal for **BCPY** and a weak fluorescence signal for **BCPM** was observed at 520 nm over a pH range from 4 to 12, which indicated that both the substrate and metabolite were stable over a wide pH range, respectively (Fig. S5). Furthermore, **BCPM** exhibited excellent performance when incubated with various potential interfering species (Fig. 2F,S6). These results indicated that **BCPM** exhibited a highly specificity for CYP2C19 even in complex bio-systems. Therefore, due to its excellent performance, **BCPM** could be used as a sensor for monitoring CYP2C19 activity.

3.3. Fluorescence imaging of CYP2C19 in living bio-samples

Subsequently, to evaluate the potential of **BCPM** for the visible analysis of CYP2C19 activity in living cells, Hek-293 and BT-549 cells were used. Prior to imaging experiments, the toxicities of **BCPM** and its metabolite **BCPY** toward Hek-293 cells were determined *via* a cell viability assay. As shown in Fig. S7, both **BCPM** and **BCPY** exhibited low cytotoxicity. When Hek-293 and BT-549 cells were stained with **BCPM** (10 μM), a strong fluorescence signal appeared (Fig. 3A). Furthermore, the fluorescence signal was strongly suppressed when a potent CYP2C19 inhibitor sulconazole was introduced, which indicating that the 'Switch-ON' of **BCPM** was triggered by intracellular CYP2C19 (Fig. 3B). **BCPM** was then used to stain the slices of mouse liver, and the 3D morphology of liver tissue could be imaged (Fig. 3C). Furthermore, the fluorescence images of liver slices were found to be consistent with immunohistochemical staining using CYP2C19 antibodies (Fig. 3D). The above results confirmed that **BCPM** could be used to monitor the activity variation of CYP2C19 even in a multidimensional biological network.

3.4. Screening of reversible and metabolism-dependent irreversible inhibitors for CYP2C19

The regulatory effect of drugs increases the variation in activity of CYP2C19, which is a causative factor for drug toxicity and side effects. As such the investigation of activity modulators for CYP2C19 is significant in the pharmaceutical industry (Furuta et al., 2010; Harmsze et al., 2011). In the present study, we attempted to construct a high-throughput screening system based on **BCPM** for the identification of direct reversible modulators and, especially, indirect and metabolism-mediated irreversible inactivators of CYP2C19, so as to achieve an efficient systematic discovery process for substances that could modulate the activity of CYP2C19 among commonly used clinical drugs, novel chemical entities and natural products. The screening strategy and flowchart to characterize the inhibition behavior of inhibitors for CYP2C19 is given in Fig. 4A. In order to integrate

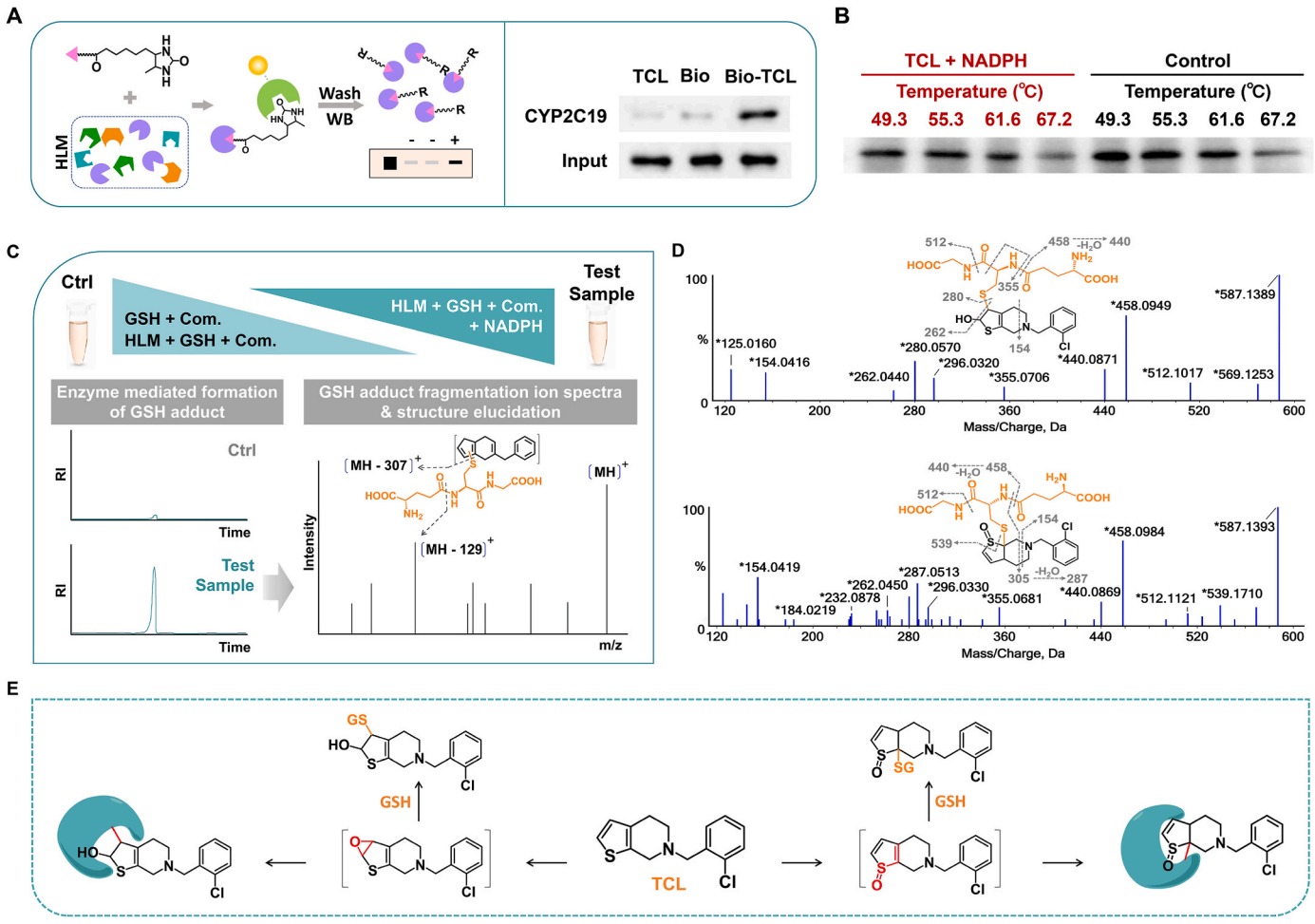


Fig. 5. The chemo-biological investigation of irreversible inactivator of CYP2C19. (A) Flowchart for pull-down assay of **Bio-TCL** with CYP2C19 in human liver microsomes (HLM, n = 3) and the representative protein bonds. (B) Thermal shift assay of TCL with CYP2C19 (n = 3). (C) Flowchart for the glutathione (GSH)-reactive intermediate scavenger assay and the corresponding MS spectra elucidation of potential adduct. (D) MS/MS spectra and proposed GSH adducts derived from TCL. (E) Proposed pathway for the formation of two GSH adducts of TCL and the corresponding potential irreversible inactivation toward CYP2C19.

irreversible inhibitor profiling with routine reversible inhibition screening, we introduced the pre-metabolism step to facilitate the biotransformation of the evaluated substances to potential reactive intermediate metabolites. Resulting in a significant decrease in residual activity of the samples treated with the NADPH-generating system when compared with the paired samples treated without NADPH-generating system indicated that the evaluated substances exhibit a metabolism-mediated inhibitory behavior and may lead to the inactivation of CYP2C19. This led to the discovery of metabolism-based inhibitors for CYP2C19, including omeprazole (OME, $C_{3,4}$), ticlopidine (TCL, $G_{5,6}$) and tanshinone I (TAN, $D_{11,12}$). Meanwhile, some direct inhibitors of CYP2C19 were identified, including efavirenz ($F_{3,4}$), sorafenib ($G_{3,4}$), lansoprazole (LAN, $F_{5,6}$), ginkgetin ($B_{7,8}$), and magnolol ($G_{9,10}$) (Fig. 4B, S8, Table S3). As such LAN (a direct inhibitor) and TCL (a indirect metabolism-mediated inhibitor) were chosen as representative compounds for the thorough analysis of metabolic inhibition using **BCPM**. The reversible inhibitor LAN exhibited a competitive inhibition pattern (Fig. 4C), and K_i was calculated to be 0.46 μM. Then, to explore the more complex metabolism-mediated interaction between TCL and CYP2C19, a limited proteolysis-coupled mass spectrometric (Lip-MS) analysis of the TCL treatment sample with its control sample was performed (Fig. 4D). The interaction between TCL, CYP2C19 and other involved CYP isoforms were investigated (Fig. 4E, S9). It was established that TCL exhibited a time- and NADPH-dependent inhibitory effect toward CYP2C19, and the K_I values were calculated to be 6.78 μM. Subsequently, dialysis experiments indicated that TCL exhibited irreversible inhibitory effects toward CYP2C19 due to the observation that the enzymatic activity failed to restore after dialysis being pre-incubated with NADPH (Fig. 4F). Co-incubation with a nucleophile or scavenger of ROS including SOD, mannitol, and glutathione (GSH) could not attenuate the inactivation of CYP2C19. However, CYP2C19 was protected from inactivation in the presence of a CYP2C19 substrate mephenytoin as evidenced by the restoration of CYP2C19 activity, when compared with TCL- and NADPH-treated samples (Fig. 4G), which indicates that the CYP2C19 substrate mephenytoin may compete with these inactivators.

The further investigation indicated that biotin-loaded TCL (**Bio-TCL**) effectively captured CYP2C19 from mixed bio-samples human liver microsomes (Fig. 5A). Furthermore, the introduction of TCL with NADPH changed the stability of the CYP2C19 protein as verified by the thermal shift assay (Fig. 5B). In order to disclose the inactivation pathway of TCL toward CYP2C19, the potential electrophilic reactive intermediate of TCL was analyzed *via* glutathione (GSH)-reactive intermediate scavenger assay (Fig. 5C). It revealed that TCL could undergo bioactivation to electrophilic thiophene-*S*-oxide and epoxide reactive intermediates (Fig. 5D), which could covalently modify CYP2C19 and cause enzymatic inactivation (Fig. 5E). These experiments identified the thiophene moiety as a key toxicophore of TCL, and provided insights into the metabolic bioactivation of TCL, inactivation mechanism of CYP2C19, and potential CYP2C19-associated drug-drug interactions.

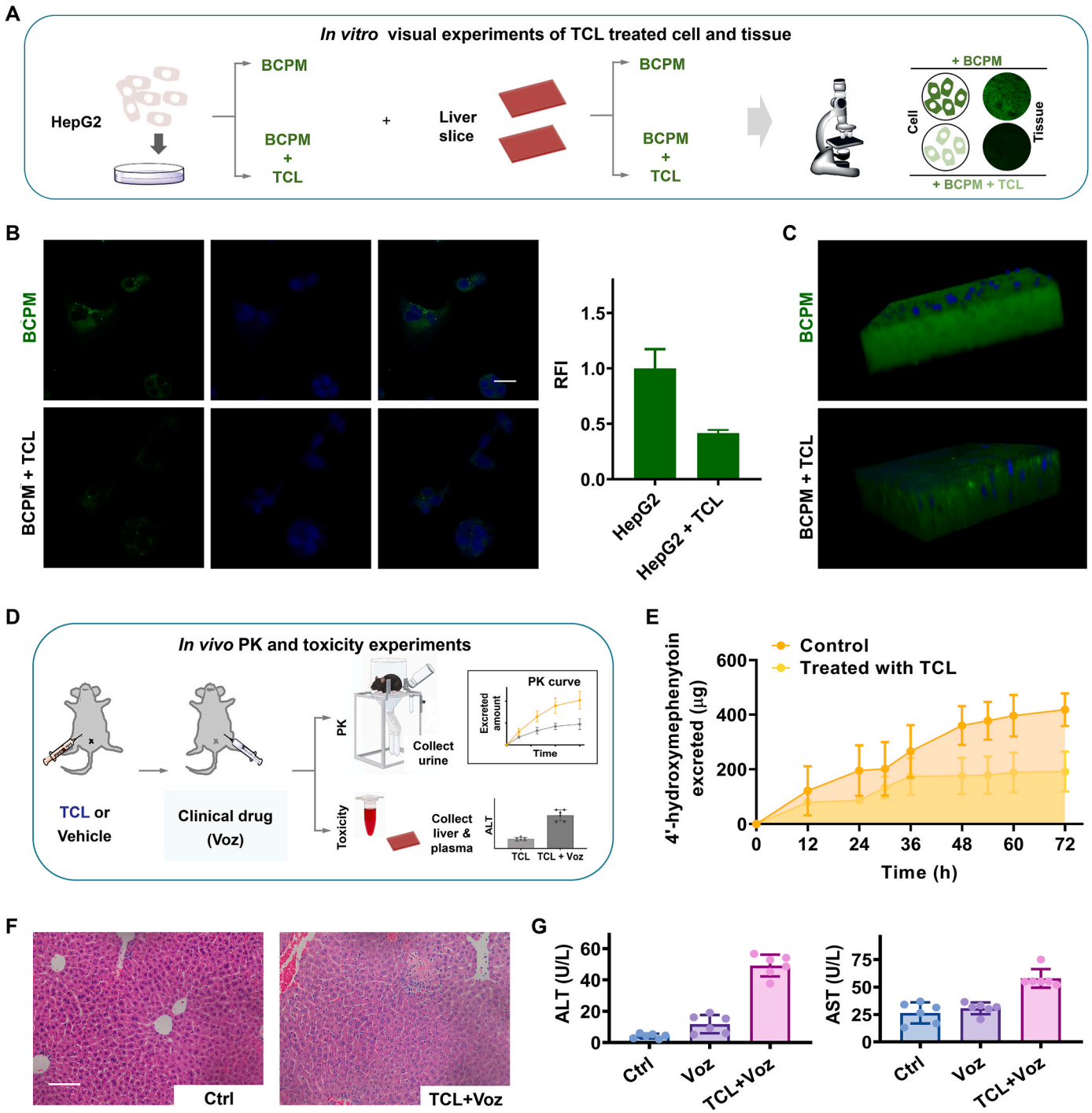


Fig. 6. The assessment of the potential drug-drug interactions induced by CYP2C19 inhibitor using TCL as an example. (A) Flowchart for a series of *in vitro* visual experiments of TCL-treated cell and tissue. (B) Fluorescence images of CYP2C19 activity in HepG2 and TCL-treated HepG2 cells using **BCPM** (n = 3). The scale bar is 25 μm. (C) Three-dimensional fluorescence images of CYP2C19 activity in control and TCL-treated mouse liver slices using **BCPM** (n = 3). (D) Flowchart for *in vivo* pharmacokinetic (PK) and hepatic injury experiments of TCL-treated mice. (E) Effects of TCL on the pharmacokinetic of mephenytoin. (F) Pathological photos of Hematoxylin and Eosin (HE) staining, The scale bar is 100 μm. (G) The alanine aminotransferase (ALT) and aspartate aminotransferase (AST) levels in serum of mice (n = 6).

3.5. The potential drug-drug interactions induced by CYP2C19 Inactivator TCL

Subsequently, a series of *in vitro* and *in vivo* experiments were conducted to systematic evaluate the potential of CYP2C19 inactivator TCL mediated drug-drug interactions (Fig. 6A). Additionally, the 'Switch-ON' of **BCPM** was strongly suppressed in liver cells and tissues, which confirmed the inhibitory effects of TCL on CYP2C19 in complex biosamples (Fig. 6B and C). Taking a step further, animal experiments were conducted to investigate the potential drug interactions and the resultant adverse drug effects induced by TCL (Fig. 6D). A pharmacokinetic study indicated that TCL resulted in decreasing the urinary excretion of the 4′-hydroxylated metabolite of CYP2C19 substrate mephenytoin in mice (Fig. 6E), indicating that TCL interfered with the CYP2C19-mediated drug metabolism *in vivo*. Furthermore, TCL could aggravate voriconazole (Voz)-induced liver damage, evidenced by

histogical analysis and sensitive indicators of liver injury (Fig. 6F and G). The above results confirmed that **BCPM** could be used for exploring CYP2C19 inhibitor associated drug-drug interactions in complex systems, facilitating guidance in the safe and effective use of medications.

4. Conclusions

In the present study, using a molecularly induced flexibility tuning strategy, we have developed a fluorescent probe **BCPM** for CYP2C19. **BCPM** exhibited excellent CYP2C19 specificity and imaging capability, making it suitable for the detection of CYP2C19 in various complex and living bio-systems. As such **BCPM** could be used to construct screening systems for discovering reversible and irreversible inhibitors of CYP2C19. **BCPM** was then used as an effective molecular tool, and could actively promote the search for CYP2C19 inhibitors, especially metabolic dependent inactivators that are hard to discover.

CRediT authorship contribution statement

Zhenhao Tian: Writing – original draft, Investigation. **Fei Yan:** Writing – original draft, Visualization, Investigation. **Yichao Su:** Investigation. **Xiaoren Zhang:** Visualization, Investigation. **Jiayue Wang:** Writing – original draft, Visualization, Investigation. **Jianing Xiao:** Investigation. **Yifei Dang:** Investigation. **Jing Ning:** Writing – review & editing, Supervision, Methodology, Conceptualization. **Lei Feng:** Writing – review & editing, Supervision, Methodology, Conceptualization. **Chengjuan Xing:** Investigation. **Xiaohong Shu:** Methodology. **Jingnan Cui:** Methodology. **Tony D. James:** Writing – review & editing, Methodology. **Xiaochi Ma:** Writing – review & editing, Supervision, Methodology, Conceptualization.

Declaration of competing interest

No author has financial or other contractual agreements that might cause conflicts of interest.

Acknowledgments

This work was supported by the National Natural Science Foundation of China (82225048, 82274359), LiaoNing Revitalization Talents Program (XLYC2203048), LiaoNing Provincial Science and Technology Plan Projects (2024JH3/10200038, and 2024-MSLH-115), Shanxi Provincial Key Research and Development Program (2024SF-GJHX-30), High-level Talents of Dalian (2023RY009), '1+X' Research Project of the Second Hospital of Dalian Medical University (DYYH2024004), the open Research Fund of Integrated Traditional Chinese and Western Medicine of Dalian Medical University (ZXY2025JC08), and the open Research Fund of the School of Chemistry and Chemical Engineering, Henan Normal University (2020ZD01 and 2021YB07).

Appendix A. Supplementary data

Supplementary data to this article can be found online at https://doi.org/10.1016/j.bios.2026.119220.

Data availability

Data will be made available on request.

References

Berge, M., Guillemain, R., Trégouet, D.A., Amrein, C., Boussaud, V., Chevalier, P., Lillo-Lelouet, A., Le Beller, C., Laurent-Puig, P., Beaune, P.H., Billaud, E.M., Loriot, M.A., 2011. Eur. J. Clin. Pharmacol. 67, 253–260.
Boyle, G.E., Sitko, K.A., Galloway, J.G., Haddox, H.K., Bianchi, A.H., Dixon, A., Wheelock, M.K., Vandi, A.J., Wang, Z.R., Thomson, R.E.S., Garge, R.K., Rettie, A.E., Rubin, A.F., Geck, R.C., Gillam, E.M.J., DeWitt, W.S., Matsen, F.A., Fowler, D.M., 2024. Genetics 228, iyae156.
Byoun, S., Heo, D.G., Lee, M., Lee, R., Li, Y., Lee, J.Y., Hong, E., Lee, W., 2026. Front. Pharmacol. 16, 1711196.
Cedrún-Morales, M., Soprano, E., Vanoni, G., Chandra, A., Iuele, H., Colella, F., Forciniti, S., Onesto, V., Grasso, G., Gigli, G., Del Mercato, L.L., 2026. J. Mater. Chem. C 14, 5607–5628.
Chen, X.L., Hu, C., Kim, H., Zhang, L.M., Zhang, Z.P.J., Liu, H.W., Yoon, J., 2026. Chem. Soc. Rev. 55, 6075–6116.
Cheng, P., Pu, K., 2024. Chem. Soc. Rev. 53, 10171–10188.
Desta, Z., Zhao, X., Shin, J.G., Flockhart, D.A., 2002. Clin. Pharmacokinet. 41, 913–958.
Donato, M.T., Jiménez, N., Castell, J.V., Gómez-Lechón, M.J., 2004. Drug Metab. Dispos. 32, 699–706.
Evans, W.E., Relling, M.V., 1999. Science 286, 487–491.
Feng, L., Ning, J., Tian, X., Wang, C., Yu, Z., Huo, X., Xie, T., Zhang, B., James, T., Ma, X., 2021. Coord. Chem. Rev. 437, 213740.
Feng, L., Tian, X., Yao, D., Yu, Z., Huo, X., Tian, Z., Ning, J., Cui, J., James, T., Ma, X., 2022. Acta Pharm. Sin. B 12, 1976–1986.
Ford, N.F., Taubert, D., 2013. J. Clin. Pharmacol. 53, 241–248.
Fricke-Galindo, I., Céspedes-Garro, C., Rodrigues-Soares, F., Naranjo, M.E., Delgado, Á., de Andrés, F., López-López, M., Peñas-Lledó, E., Llerena, A., 2016. Pharmacogenomics J. 16, 113–123.
Furuta, T., Iwaki, T., Umemura, K., 2010. Br. J. Clin. Pharmacol. 70, 383–392.
Goldstein, J.A., 2001. Br. J. Clin. Pharmacol. 52, 349–355.
Gougis, P., Hilmi, M., Geraud, A., Mir, O., Funck-Brentano, C., 2021. Crit. Rev. Oncol. Hematol. 166, 103342.
Grasso, G., Colella, F., Forciniti, S., Onesto, V., Iuele, H., Siciliano, A.C., Carnevali, F., Chandra, A., Gigli, G., Del Mercato, L.L., 2023. Nanoscale Adv. 5, 4311–4336.
Guengerich, F.P., 2020. Toxicol. Res. 37, 1–23.
Guengerich, F.P., 2024. Drug Metab. Dispos. 52, 493–497.
Harmsze, A.M., van Werkum, J.W., Souverein, P.C., Breet, N.J., Bouman, H.J., Hackeng, C.M., Ruven, H.J., ten Berg, J.M., Klungel, O.H., de Boer, A., Deneer, V.H., 2011. J. Thromb. Haemostasis 9, 1892–1901.
He, R.J., Tian, Z.H., Huang, J., Sun, M.R., Wei, F., Li, C.Y., Zeng, H.R., Zhang, F., Guan, X. Q., Feng, Y., Meng, X.M., Yang, H., Ge, G.B., 2023. J. Med. Chem. 66, 6743–6755.
Hicks, J.K., Sangkuhl, K., Swen, J.J., Ellingrod, V.L., Müller, D.J., Shimoda, K., Bishop, J. R., Kharasch, E.D., Skaar, T.C., Gaedigk, A., Dunnenberger, H.M., Klein, T.E., Caudle, K.E., Stingl, J.C., 2017. Clin. Pharmacol. Ther. 102, 37–44.
Hicks, J.K., Swen, J.J., Thorn, C.F., Sangkuhl, K., Kharasch, E.D., Ellingrod, V.L., Skaar, T.C., Müller, D.J., Gaedigk, A., Stingl, J.C., 2013. Clin. Pharmacol. Ther. 93, 402–408.
Jiang, M., You, J.H., 2015. Expert Opin. Pharmacother. 16, 771–779.
Juvonen, R.O., Ahinko, M., Huuskonen, J., Raunio, H., Pentikäinen, O.T., 2019. Xenobiotica 49, 1015–1024.
Kalgutkar, A.S., Obach, R.S., Maurer, T.S., 2007. Curr. Drug Metabol. 8, 407–447.
Lee, J.Y., Lee, S.Y., Oh, S.J., Lee, K.H., Jung, Y.S., Kim, S.K., 2012. Chem. Biol. Interact. 198, 49–56.
Li, H., Lu, Q.Y., Xu, B.M., Li, A.Q., Fang, J., He, X.S., Bian, X.L., 2026. J. Antimicrob. Chemother. 81, dkag065.
Lin, J.H., Lu, A.Y., 1998. Clin. Pharmacokinet. 35, 361–390.
Mega, J.L., Close, S.L., Wiviott, S.D., Shen, L., Hockett, R.D., Brandt, J.T., Walker, J.R., Antman, E.M., Macias, W., Braunwald, E., Sabatine, M.S., 2009. N. Engl. J. Med. 360, 354–362.
Mu, R.J., Gao, J.J., Wang, X.L., Ling, J., Hu, N., Yang, H.Y., 2025. Pharmaceutics 17, 1582.
Ning, J., Tian, Z., Wang, J., Wang, B., Tian, X., Yu, Z., Huo, X., Feng, L., Cui, J., James, T., Ma, X., 2022. Angew. Chem., Int. Ed. 61, e202113191.
Ning, J., Tian, Z., Wang, J., Yan, F., Shi, C., Zhang, S., Feng, L., Shu, X., Cui, J., James, T., Ma, X., 2024. Angew. Chem., Int. Ed. 63, e202409217.
Niwa, T., Murayama, N., Emoto, C., Yamazaki, H., 2008. Curr. Drug Metabol. 9, 20–33.
Rendic, S., Guengerich, F.P., 2015. Chem. Res. Toxicol. 28, 38–42.
Roichman, A., Zuo, Q., Hwang, S., Lu, W., Cordova, R.A., MacArthur, M.R., Boyer, J.A., Mitchell, S.J., Powers, J., Koval, S.A., Hunter, C.J., Rijmers, J., Ryseck, R.P., AbuSalim, J.E., Chatterjee, S., Lee, W.D., Xu, X., Xing, X., Chen, Z., Zeng, X., Marwaha, S., McBride, M.J., Guo, J.Y., Kang, Y., Donia, M.S., Rabinowitz, J.D., 2025. Cell 188, 3065–3080.
Salminen, K.A., Leppänen, J., Venäläinen, J.I., Pasanen, M., Auriola, S., Juvonen, R.O., Raunio, H., 2011. Drug Metab. Dispos. 39, 412–418.
Sudsakorn, S., Skell, J., Williams, D.A., O'Shea, T.J., Liu, H., 2007. Drug Metab. Dispos. 35, 841–847.
Sychev, D.A., Ashraf, G.M., Svistunov, A.A., Maksimov, M.L., Tarasov, V.V., Chubarev, V. N., Otdelenov, V.A., Denisenko, N.P., Barreto, G.E., Aliev, G., 2018. Drug Des. Dev. Ther. 12, 1147–1156.
Tang, L.W.T., Wei, W., Verma, R.K., Koh, S.K., Zhou, L., Fan, H., Chan, E.C.Y., 2022. Drug Metab. Dispos. 50, 529–540.
Thuy, H.M., Sugimoto, M., Quang, P.M.N., Yamaoka, Y., 2026. Expert Rev. Clin. Pharmacol. 19, 133–150.
Wallentin, L., James, S., Storey, R.F., Armstrong, M., Barratt, B.J., Horrow, J., Husted, S., Katus, H., Steg, P.G., Shah, S.H., Becker, R.C., 2010. PLATO investigators. Lancet 376, 1320–1328.
Wang, F.Y., Wei, L., Wang, P., Chen, W.C., Chen, Z.J., Zhou, Z.Q., Zhu, G.H., Gong, Q., Qin, L.P., Yang, L., Ge, G.B., Wang, P., 2026. Biosens. Bioelectron. 298, 118409.
Williams, J.A., Ring, B.J., Cantrell, V.E., Jones, D.R., Eckstein, J., Ruterbories, K., Hamman, M.A., Hall, S.D., Wrighton, S.A., 2002. Drug Metab. Dispos. 30, 883–891.
Wu, X., Wang, R., Kwon, N., Ma, H., Yoon, J., 2022. Chem. Soc. Rev. 51, 450–463.
Xu, W.Y., Zhang, Y.F., Ji, L.X., Chen, Y.L., Zhao, D., 2026. J. Fluoresc. 36, 2337–2346.

Yan, F., He, S., Han, X., Wang, J., Tian, X., Wang, C., James, T., Cui, J., Ma, X., Feng, L., 2022. Biosens. Bioelectron. 216, 114606.
Yang, S., Wang, L., Wu, J., Liu, T., Pei, S., Zhou, Q., Wu, Q., 2025. Chembiochem 26, e202500278.
Zanger, U.M., Schwab, M., 2013. Pharmacol. Ther. 138, 103–141.
Zhou, Y., Li, J.H., Baryshnikov, G., Tu, Y.Q., 2022. J. Chem. Inf. Model. 62, 6172–6181.